NANO LETTERS

Letter

pubs.acs.org/NanoLett

# Local Heating with Lithographically Fabricated Plasmonic Titanium Nitride Nanoparticles

Urcan Guler,[†] Justus C. Ndukaife,[†,‡] Gururaj V. Naik,[†] A. G. Agwu Nnanna,[‡] Alexander V. Kildishev,[†] Vladimir M. Shalaev,[†] and Alexandra Boltasseva*[,†,§]

[†]School of Electrical and Computer Engineering and Birck Nanotechnology Center, Purdue University, West Lafayette, Indiana 47907, United States

[‡]Water Institute, Purdue University Calumet, Hammond, Indiana 46323, United States

[§]DTU Fotonik, Department of Photonics Engineering, Technical University of Denmark, Lyngby DK-2800, Denmark

Supporting Information

**ABSTRACT:** Titanium nitride is considered a promising alternative plasmonic material and is known to exhibit localized surface plasmon resonances within the near-infrared biological transparency window. Here, local heating efficiencies of disk-shaped nanoparticles made of titanium nitride and gold are compared in the visible and near-infrared regions numerically and experimentally with samples fabricated using e-beam lithography. Results show that plasmonic titanium nitride nanodisks are efficient local heat sources and outperform gold nanodisks in the biological transparency window, dispensing the need for complex particle geometries.

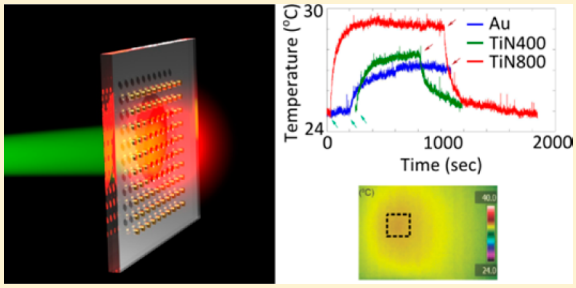


**KEYWORDS:** *LSPR, plasmonic heating, TiN nanoparticle, photothermal effect, photodynamic therapy, biomaterials*

Plasmonics has been a hot topic for the last two decades with innumerable promising results in several different application areas.[1,2] Although the field has been investigated widely by many researchers from all around the world, recent research trends still follow the early examples of this field. For instance, gold (Au) and silver (Ag) are the most popular choices as plasmonic materials. However, it was shown that an ancient example of plasmonics, the Lycurgus Cup, contains silver−gold alloyed nanoparticles. This reveals the fact that the search for alternative plasmonic materials is as old as the history of plasmonics itself.[3] With the significant improvement of nanoscale fabrication and characterization techniques, the initial tendency of the scientific community was to examine noble metals as plasmonic materials due to their suitable dielectric functions in the visible region of the electromagnetic spectrum.[4−6] As the understanding of physical mechanisms has progressed, researchers are now working to find, or synthesize, the optimum materials for individual application areas and related spectral windows.[7−9]

Titanium nitride (TiN) is known to exhibit plasmonic behavior.[10−14] Owing to the similarities of its optical properties to those of Au with additional significant advantages such as low cost, thermal stability, and compatibility with silicon nanofabrication techniques, TiN draws attention as a promising alternative plasmonic material.[15,16] Recently, we have shown that near-field enhancement due to the localized surface plasmon resonance (LSPR) in nitride plasmonic materials is comparable to Au, and the dipolar resonance peak naturally occurs at the border of the visible and the near-infrared regions.[17] The LSPR spectral position of small, spherical TiN nanoparticles matches very well with the biological transparency window where plasmonics-based biological research is carried out.[18,19] Currently, these applications are dominated by Au nanoparticles because of their biocompatibility and relatively good plasmonic properties in the visible region.[20] However, gold's LSPR peaks occur at shorter wavelengths and researchers have worked to redshift the resonance into the biological window by using complex structures.[21,22]

Beyond the biological applications, local heating with plasmonic nanoparticles is considered to be a promising method for several other applications ranging from catalysis to heat-assisted magnetic recording.[23−27] TiN nanoparticles are promising alternatives to replace noble metals due to their increased heating efficiencies over Au in the red and near-infrared regions and provide additional exciting properties such as high melting temperature, chemical stability, mechanical durability, and compatibility to CMOS technology. In addition, plasmonic TiN nanoparticles with simple shapes would be favored when compared to complex metal nanostructures. Shape-tuned metal nanostructures may bring additional difficulties due to their structural complexities. For example, using nanorods with large aspect ratios results in a polarization dependent response of particles and would reduce the total efficiency due to lack of orientation control over the particles in

**Received:** September 7, 2013
**Revised:** November 23, 2013
**Published:** November 26, 2013

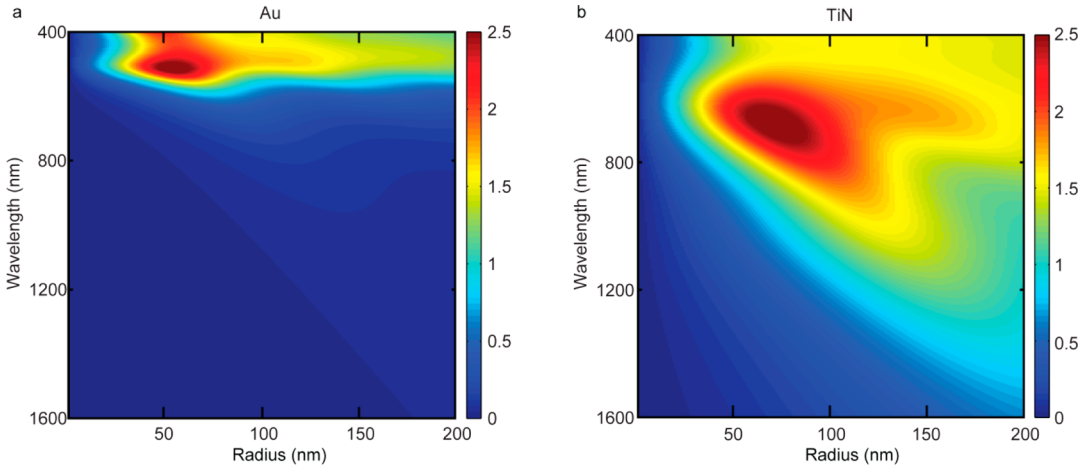


**Figure 1.** Absorption efficiencies of (a) Au and (b) TiN spherical nanoparticles obtained from Mie calculations. Peak values for both materials are equal but the spectral position is at 520 nm for Au and 700 nm for TiN. A broad resonance with equivalent strength located very close to the biological transparency window, makes TiN a promising plasmonic material for biological applications.

many applications. Sharp edges in complex-shaped particles would be exposed to higher field intensities and temperatures, resulting in shape deformations, which will eventually degrade the performance.

Local heating with plasmonic nanoparticles is based on the idea of delivering energy with electromagnetic waves to the region of interest, where plasmonic nanoparticles concentrate light and generate heat within a confined volume through ohmic losses at the resonance wavelengths.[18,28] The heat generated by a nanoparticle is known to be proportional to the intensity of the illuminating light where the proportionality constant is the absorption efficiency of the particle, defined as the absorption cross-section normalized by the geometrical cross-sectional area of the particle under illumination.[29] Thus, assuming a constant illumination intensity, the absorption efficiency of the particle can be used as a figure of merit (FOM) for comparison purposes. Among the parameters affecting the absorption efficiency of a plasmonic particle, size and shape have been extensively studied.[30,31] Other important parameters that affect the absorption efficiency are the optical constants of the nanoparticle that are dependent on the plasmonic material and the illumination wavelength.

In this Letter, we compare TiN and Au nanoparticles within the perspectives of local heating for biological and other important applications and show that TiN performs better than Au in the spectral range that includes the biological transparency window. Electron beam lithography (EBL) is used for the fabrication of Au and TiN nanoparticle arrays ranging in size from 60 to 180 nm in diameter with varying lattice constants. They are deposited on sapphire substrates, which have a thermal conductivity of ($\kappa$ = 42 W/m × K).[36] Au samples are deposited with electron beam deposition while TiN samples are deposited with dc reactive magnetron sputtering at 400 and 800 °C. Spectroscopic ellipsometry (V-VASE, J. A. Woollam Co.) is used for the transmittance measurements of the nanoparticle arrays and for the dielectric constant retrieval from thin films grown simultaneously with nanoparticles. Retrieved optical constants are employed in numerical simulations with the finite element method (FEM) based commercial software (COMSOL Multiphysics). Nanodisk arrays are illuminated with a laser beam at an 800 nm wavelength and heat generation is observed with a thermal camera, FLIR A320, by measuring the temperature change in the substrate. Details of the experimental methods are given in the Supporting Information.

A simple and efficient method for comparing different materials for local heating applications is to calculate absorption efficiency of spherical nanoparticles of varying sizes through the Mie scattering formulation.[32] Au and TiN optical constants retrieved from thin films are employed in the calculations where parameter sweep over the particle radius and excitation wavelength are performed. Size effects on the permittivities are neglected since the dimensions of the particles examined in this work are relatively large. The absorption efficiencies obtained from Mie calculations are plotted in Figure 1. The well-known behavior of the reference material, Au, is evident in Figure 1a, where the LSPR peak is located around 520 nm with an optimal particle radius around 55 nm. The peak efficiency at these parameters is around 2.5. As expected, Au nanoparticles exhibit a narrow peak that for most of the applications dictate precise control on the size dispersion of particles.[33] In order to obtain a strong response from Au nanoparticles in the biological transparency window, it is a common practice to use particles with large aspect ratios and complex shapes.[21,34] However, as the size of the particle increases, higher order modes become supported and interference effects between multiple modes reduce the efficiency. TiN nanoparticles, on the other hand, exhibit a broad resonance peak located around 700 nm with maximum absorption efficiency around 2.5, identical to the Au peak value. A broad, dipolar peak of comparable strength occurring at wavelengths closer to the biological transparency window is a significant advantage of TiN nanoparticles over Au. From the initial comparison based on Mie calculations, one can claim that TiN nanoparticles of simple geometries with reduced restrictions on the size-dispersion can provide better efficiencies for heating applications when compared to Au.

In order to verify these calculations, Au and TiN nanodisk arrays with identical shapes are fabricated using the EBL technique. Au samples are prepared by electron beam deposition while TiN samples are deposited using dc reactive magnetron sputtering at substrate temperatures of 400 and 800 °C.[16] TiN nanodisks grown at different temperatures are examined due to the nonstoichiometric nature of the material.[35]


dx.doi.org/10.1021/nl4033457 | Nano Lett. 2013, 13, 6078−6083

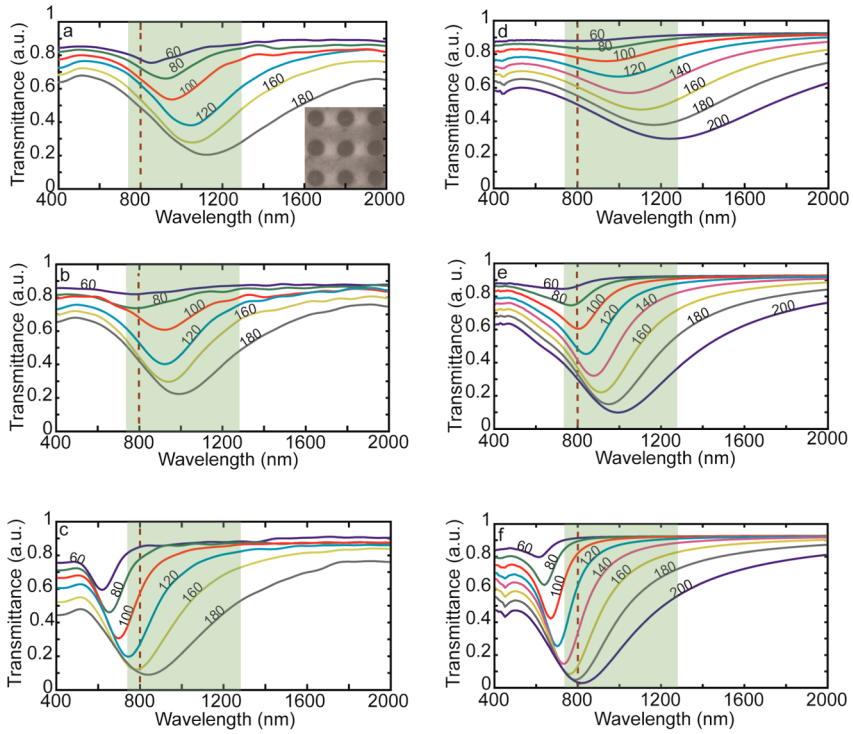


**Figure 2.** Transmittance spectra for 30 nm thick nanodisk arrays of TiN grown at (a) 400 °C, (b) 800 °C, and (c) Au. The spectral position of the transmittance dips due to the extinction of particles indicates that TiN nanodisks exhibit plasmonic resonances throughout the biological transparency window (green regions). The plasmonic peaks of Au nanoparticles with smaller sizes are located at relatively short wavelengths, and larger particles are required to reach the spectral region of interest. (d–f) The simulation results of the transmittance through the arrays of the particles match well with the experimental data allowing the following simulation based discussions on absorption efficiencies. The dashed line shows the excitation wavelength used for the heating experiments in this work. The inset shows EBL patterned TiN nanoparticles deposited at 400 °C.

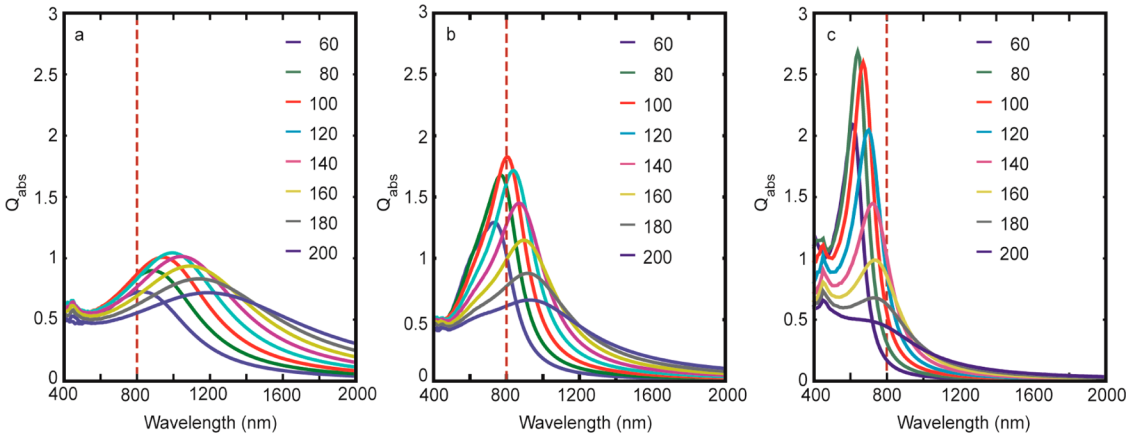


**Figure 3.** Simulated absorption efficiencies of nanodisks for TiN grown at (a) 400 °C, (b) 800 °C, and (c) Au. Broad resonance peaks throughout the biological transparency window obtained from nanodisks of TiN suggest that high local heating efficiencies can be reached. The dashed line shows the excitation wavelength used for the heating experiments in this work.

Samples grown at higher temperatures are known to be more metallic (larger magnitude of the real part of permittivity) when compared to the samples grown at lower temperatures. The nanodisks range in size from 60 to 180 nm with varying lattice constants on sapphire substrates, which has a thermal conductivity of ($\kappa$ = 42 W/m × K).[36] The LSPR peak positions of these particles are determined from the extinction dips in the optical transmittance data obtained from spectroscopic ellipsometry. Thin films grown under the same deposition conditions as with the nanoparticles were characterized with ellipsometry and retrieved optical constants were used in subsequent 3D FEM simulations. Figure 2a–c shows the experimental transmittance data of the nanoparticle arrays of TiN grown at two different temperatures, 400 °C (a) and 800 °C (b), and Au as the reference material. A comparison between TiN nanoparticles grown at different temperatures shows that due to the nonstoichiometric nature of the material the resonance behavior of these particles can be tuned by varying the growth parameters. It is evident that the biological transparency window, highlighted with green in the figure, can be covered by the LSPR peaks of TiN nanoparticles with varying sizes and growth conditions. On the other hand, transmittance data from Au nanodisks have dips starting at 600 nm with the smallest particles and increasing up to 850 nm with


dx.doi.org/10.1021/nl4033457 | *Nano Lett.* 2013, 13, 6078–6083

larger particles. Figure 2d–f shows the simulated transmittance data of the nanoparticle arrays that agree quite well with the experimental results. Although the spectral position and strength of the extinction peaks provides important details about the performance of nanoparticles, the crucial FOM for local heating applications is the absorption efficiency of the particles as mentioned earlier. It should be noted that a stronger resonance dip in the transmittance spectra of Au sample is due to the larger extinction efficiency of these particles, which is the sum of absorption and scattering. However, it is not easy to experimentally compare the absorption efficiencies of small nanoparticles with high precision. Since there is good agreement between numerically simulated and experimentally measured transmittance data presented in Figure 2, the absorption efficiencies of the nanoparticles are determined via numerical simulations.

Absorption efficiencies calculated from FEM simulations of nanodisk arrays are presented in Figure 3 for TiN and Au. Figure 3a,b shows the absorption efficiencies of TiN nanodisks of varying sizes grown at 400 and 800 °C, respectively. As mentioned, due to the nonstoichiometric nature of TiN, both spectral position and strength of the resonance depends on the growth temperature, and their efficiencies vary accordingly. For TiN nanodisks grown at 400 °C, the smallest particles with a diameter of 60 nm have their peak absorption efficiency at a wavelength of 800 nm, while the largest particles with a diameter of 200 nm have their peak absorption efficiency at a wavelength of 1200 nm. These wavelengths are the limits of the biological transparency window. Nanodisks with a size of 120 nm provide the best absorption efficiency at a wavelength of 1000 nm. Although the efficiency decreases with increasing particle size after the optimum size of 120 nm, one can see that 200 nm particles provide a broad efficiency peak, which covers the entire window and weakly varies with wavelength when compared to smaller particles. Particles grown at 800 °C have stronger and sharper efficiency peaks varying between 700 to 1000 nm with increasing dimensions. The highest absorption efficiency is obtained with 100 nm disks at the wavelength of 800 nm. These particles provide relatively high absorption efficiencies up to 1000 nm, which makes them favorable for biological applications. Optical constants retrieved from the reference thin film samples for each material are provided in Figure S1 of the Supporting Information. The TiN sample grown at 800 °C exhibits a more metallic behavior that results in a blue-shifted plasmonic peak when compared to TiN deposited at 400 °C. Figure 3c shows the absorption efficiencies for Au nanoparticles where strong but spectrally narrow peaks are observed. Not surprisingly, the spectral positions of these particles are at shorter wavelengths and can hardly match the lower limit of biological transparency window, even with large diameter particles. However, large particles have poor absorption efficiencies lending to the use of more complicated geometries, such as nanoshells, to obtain the desired performance.[37] In the case of Au, the efficiency of 200 nm particles is severely degraded and the resulting peak is hardly visible. A comparison of the absorption efficiencies for nanodisks shows that although Au particles provide high peak values for small wavelengths, they are not as efficient as TiN nanoparticles of similar sizes in the red and near-infrared regions, including the biological transparency window. Increasing the particle size redshifts the resonance position but reduces the absorption efficiency. Consequently, TiN particles have the potential to provide higher energy conversion efficiencies at the nanometer scale when compared to Au due to their LSPR being intrinsically located near the biological window.

In this work, heating efficiencies of nanoparticles are also examined experimentally. Sapphire substrates with arrays of Au and TiN nanoparticles are imaged with a FLIR infrared camera with a pitch size of 25 $\mu$m and illuminated with a laser at 800 nm. Figure 4a provides an illustration of the experiment while

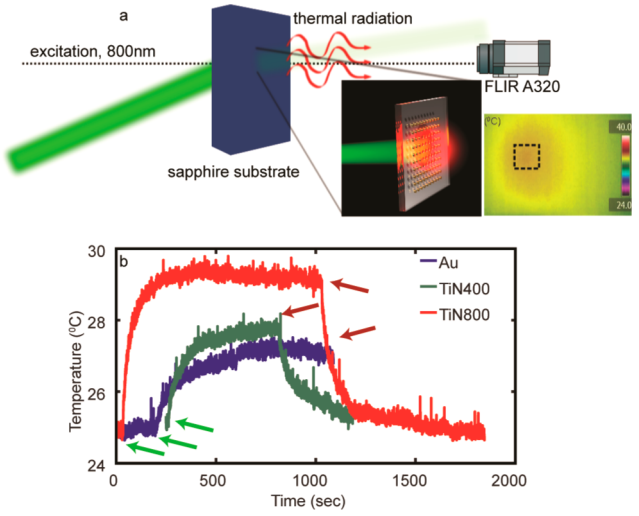


**Figure 4.** (a) Illustration of nanodisk arrays illuminated with laser light at 800 nm. (Inset) Steady-state thermal image of the sapphire substrate with illuminated TiN nanoparticles. The dashed rectangle shows the position of the EBL fabricated nanodisk array. (b) Time-dependent temperature of the sapphire substrate heated by the plasmonic nanodisks excited with 800 nm laser light. TiN nanodisks grown at 800 °C clearly perform better than Au nanoparticles. Green and red arrows indicate the time the laser is turned on and off for each sample, respectively.

the inset shows an image obtained in the steady state of the system where the location of the nanodisk array heat source is designated by a dashed rectangle. As an excitation source in the biological transparency window, a Ti:sapphire regenerative amplifier with emission at 800 nm is chosen. Only the largest particles are examined at this step for two reasons: (1) in this wavelength region, the resonance from Au particles is observed only for large particles (180 nm) and (2) the larger surface coverage provides increased heating that can be observed with the thermal camera. Substrates are heated by the optically excited nanodisks and the time dependent average temperature change of the substrate was recorded. Figure 4b shows the temperature averaged over the area of nanodisk arrays located on sapphire substrate. Owing to their high thermal conductivities (42W/m × K), sapphire substrates act as strong heat sinks and prevent reaching high temperatures. Using a low thermal conductivity substrate such as glass would yield higher temperature readings. However, a glass substrate was not used in this work because of its low melting point when compared to the high temperatures used for TiN deposition. When the laser is turned on, the temperature increase observed from the samples follows the previously reported experimental and theoretical results for a system consisting of plasmonic nanoparticles as heat sources and the host medium acting as an external reservoir.[20] Although the excitation wavelength corresponds to the extinction peak of the Au nanodisks, the


dx.doi.org/10.1021/nl4033457 | Nano Lett. 2013, 13, 6078–6083

steady-state temperature increase obtained from Au arrays is low when compared to that of TiN nanoparticles grown at 400 and 800 °C. Extinction dips observed in the transmittance data presented in Figure 2 reveal that TiN particles of 180 nm size grown at 400 and 800 °C are expected to provide better heating efficiencies when excited at wavelengths around 1100 and 1000 nm, respectively. Also, the numerical data for the absorption efficiencies predict that TiN grown at 800 °C should give better heating performance at the excitation wavelength of 800 nm. This is in agreement with the larger experimentally observed temperature increase from the TiN sample grown at 800 °C. Although the illuminating light is off the resonance peak for TiN nanodisks grown at 800 °C, these particles still provide a temperature increase of 4 °C, which is 2 times the heating obtained from Au nanoparticles of same size. Densely packed TiN nanoparticles of smaller sizes excited with 800 nm light will provide a much higher temperature increase due to the spectral match of the resonance peak wavelength with the excitation source.

In this work, we have experimentally demonstrated the superior performance of TiN over Au for local heating applications with lithographically fabricated nanodisks. However, large-scale EBL is not feasible method to generate TiN nanoparticles. Therefore, obtaining plasmonic TiN nanoparticles through chemical methods would be of high interest to researchers in the field of plasmonics. Although synthesis of TiN powders has been a hot topic due to above-mentioned superior physical properties of the material, plasmonic properties have not been reported so far. A wide range of methods to generate TiN powders have been investigated including ammonolysis of titanium dioxide nanoparticles,[38] vapor synthesis,[39] benzene-thermal route,[40] urea route,[41] mechanical ball milling,[42] and laser ablation.[43] Our current research is focused on fabricating plasmonic TiN powders and promising initial results have been obtained. The development of a chemical synthesis method for plasmonic TiN nanoparticles would also stimulate the studies on surface chemistry and potential toxicity of nanostructured TiN, which is already a widely used material in biomedical applications.[44−46]

In conclusion, TiN nanodisks were studied in the scope of local heating applications and their heating efficiency was compared to the widely used Au nanodisks. Both Mie calculations and FEM simulations suggest that TiN nanoparticles can perform better than Au in the biological transparency window due to the spectral match of the dipolar resonances to the region of interest. Particles with identical geometries fabricated via EBL are compared through transmittance and heating experiments in order to verify the numerical findings. Experiments reveal that TiN nanodisks can outperform Au nanodisks of same geometrical parameters and eliminate the need for complex-shaped metal nanostructures in practical applications. Considering the fact that TiN is a biocompatible, CMOS compatible, and durable material with a high melting point, our results prove that TiN is a promising material candidate for many areas such as biological and medical applications, energy harvesting, heat-assisted magnetic recording, and others.

**Materials and Methods.** *Sample Fabrication.* EBL is used for nanodisk fabrication due to the high accuracy of the technique on the geometry of the features. Au samples were deposited on a sapphire substrate with electron beam evaporation and TiN samples were deposited with DC reactive magnetron sputtering from a Ti target under 4 sccm Ar and 6 sccm $N_2$ flow. Two growth temperatures were used for TiN samples, 400 and 800 °C. The deposition rate is approximated as 21 Å/min and the final thickness of the structures were measured as 30 nm with atomic force microscopy (Veeco Dimension 3100 AFM). Because of the high-temperature growth of TiN samples, an 80 nm thick Cr lift-off layer was added to the standard lithography process. The nanoparticle pattern was transferred from ZEP 520A resist to Cr layer by use of reactive ion etching (Panasonic E620 Etcher). After TiN deposition, the Cr lift-off layer was removed with wet etching (Cyantek CR-7). The same procedure is followed for Au samples in order to ensure shape consistency. During each deposition, a thin film sample was grown as a reference for dielectric constant retrieval.

*Optical Measurements.* The dielectric functions of each material used in this work were retrieved from thin films by use of a variable angle spectroscopic ellipsometer (V-VASE, J. A. Woollam Co.). The Drude-Lorentz model was used for data retrieval; details of data fit are given in the Supporting Information. The same ellipsometer setup was employed for transmittance measurements with optional focusing probes, which allow examination of lithographic samples with dimensions down to 500 $\mu$m × 500 $\mu$m.

*Thermal Measurements.* Samples were excited with 650 mW of weakly focused laser light from a Ti:sapphire regenerative amplifier at a wavelength of 800 nm. Illumination was performed from backside and at a slight angle in order to prevent damage to the infrared camera. Heated samples were imaged with a thermal camera (FLIR A320). The substrate temperature was averaged over the area of the nanoparticle arrays for each sample, resulting in a time-dependent temperature line plot. The laser source was turned off after reaching a steady state for each sample. All samples were placed on a fixed holder on the optical axis in order to ensure constant laser intensity for each sample.

## ■ ASSOCIATED CONTENT

### Ⓢ Supporting Information

The dielectric functions retrieved from thin film samples and included in FEM simulations are presented; oscillator model and fit parameters are provided. The absorption efficiencies for spherical nanoparticles of TiN and Au located in water are given. SEM images of Au and TiN samples are given. The thermal measurement presented in Figure 4 of main text was simulated for TiN nanoparticles grown at 800 °C and compared to experimental result in Figure S4. This material is available free of charge via the Internet at http://pubs.acs.org.

## ■ AUTHOR INFORMATION

### Corresponding Author

*E-mail: aeb@purdue.edu.

### Notes

The authors declare no competing financial interest.

## ■ ACKNOWLEDGMENTS

The authors acknowledge support from the following grants: ONR-MURI Grant N00014-10-1-0942, ARO Grant 57981-PH (W911NF-11-1-0359), and NSF MRSEC Grant DMR-1120923. J.N. also acknowledges financial assistance from Purdue Calumet Water Institute. We are thankful to Nathaniel Kinsey for the help in preparation of this manuscript.

## REFERENCES


(1) Barnes, W. L.; Dereux, A.; Ebbesen, T. W. *Nature* **2003**, *424* (6950), 824−830.
(2) Atwater, H. A. *Sci. Am.* **2007**, *296* (4), 56−63.
(3) Freestone, I.; Meeks, N.; Sax, M.; Higgitt, C. *Gold Bull.* **2007**, *40* (4), 270−277.
(4) Lal, S.; Link, S.; Halas, N. J. *Nat. Photonics* **2007**, *1* (11), 641−648.
(5) Maier, S. A. *Plasmonics: Fundamentals and Applications: Fundamentals and Applications*; Springer: New York, 2007.
(6) Schuller, J. A.; Barnard, E. S.; Cai, W.; Jun, Y. C.; White, J. S.; Brongersma, M. L. *Nat. Mater.* **2010**, *9* (3), 193−204.
(7) Blaber, M. G.; Arnold, M. D.; Ford, M. J. *J. Phys. Chem. C* **2009**, *113* (8), 3041−3045.
(8) Boltasseva, A.; Atwater, H. A. *Science* **2011**, *331* (6015), 290−291.
(9) Naik, G. V.; Shalaev, V. M.; Boltasseva, A. *Adv. Mater.* **2013**, *25* (24), 3264−3294.
(10) Steinmüller-Nethl, D.; Kovacs, R.; Gornik, E.; Rödhammer, P. *Thin Solid Films* **1994**, *237* (1), 277−281.
(11) Hibbins, A. P.; Sambles, J. R.; Lawrence, C. R. *J. Modern Opt.* **1998**, *45* (10), 2051−2062.
(12) Reinholdt, A.; Pecenka, R.; Pinchuk, A.; Runte, S.; Stepanov, A. L.; Weirich, T. E.; Kreibig, U. *Eur. Phys. J. D* **2004**, *31* (1), 69−76.
(13) Cortie, M. B.; Giddings, J.; Dowd, A. *Nanotechnology* **2010**, *21* (11), 115201.
(14) Chen, N. C.; Lien, W. C.; Liu, C. R.; Huang, Y. L.; Lin, Y. R.; Chou, C.; Chang, S. Y.; Ho, C. W. *J. Appl. Phys.* **2011**, *109* (4), 043104.
(15) Naik, G. V.; Kim, J.; Boltasseva, A. *Opt. Mater. Express* **2011**, *1* (6), 1090−1099.
(16) Naik, G. V.; Schroeder, J. L.; Ni, X.; Kildishev, A. V.; Sands, T. D.; Boltasseva, A. *Opt. Mater. Express* **2012**, *2* (4), 478−489.
(17) Guler, U.; Naik, G.; Boltasseva, A.; Shalaev, V.; Kildishev, A. *Appl. Phys. B: Lasers Opt.* **2012**, *107* (2), 285−291.
(18) Cole, J. R.; Mirin, N. A.; Knight, M. W.; Goodrich, G. P.; Halas, N. J. *J. Phys. Chem. C* **2009**, *113* (28), 12090−12094.
(19) Smith, A. M.; Mancini, M. C.; Nie, S. *Nat Nanotechnol.* **2009**, *4* (11), 710−711.
(20) Richardson, H. H.; Carlson, M. T.; Tandler, P. J.; Hernandez, P.; Govorov, A. O. *Nano Lett* **2009**, *9* (3), 1139−1146.
(21) Baffou, G.; Quidant, R. *Laser Photonics Rev.* **2013**, *7* (2), 171−187.
(22) Halas, N. *MRS Bull.* **2005**, *30* (05), 362−367.
(23) Adleman, J. R.; Boyd, D. A.; Goodwin, D. G.; Psaltis, D. *Nano Lett* **2009**, *9* (12), 4417−4423.
(24) Hung, W. H.; Aykol, M.; Valley, D.; Hou, W.; Cronin, S. B. *Nano Lett* **2010**, *10* (4), 1314−1318.
(25) Boyd, D. A.; Greengard, L.; Brongersma, M.; El-Naggar, M. Y.; Goodwin, D. G. *Nano Lett* **2006**, *6* (11), 2592−2597.
(26) Neumann, O.; Urban, A. S.; Day, J.; Lal, S.; Nordlander, P.; Halas, N. J. *ACS Nano* **2012**, *7* (1), 42−49.
(27) Kryder, M. H.; Gage, E. C.; McDaniel, T. W.; Challener, W. A.; Rottmayer, R. E.; Ganping, J.; Hsia, Y.-T.; Erden, M. F. *Proc. IEEE* **2008**, *96* (11), 1810−1835.
(28) Baffou, G.; Quidant, R.; Garcia de Abajo, F. J. *ACS Nano* **2010**, *4* (2), 709−716.
(29) Bohren, C.; Huffman, D. *Absorption and Scattering of Light by Small Particles*; Wiley-VCH: New York, 1998.
(30) Govorov, A. O.; Richardson, H. H. *Nano Today* **2007**, *2* (1), 30−38.
(31) Baffou, G.; Girard, C.; Quidant, R. *Phys. Rev. Lett.* **2010**, *104* (13), 136805.
(32) Mie, G. *Ann. Phys.* **1908**, *330* (3), 377−445.
(33) Ye, X.; Jin, L.; Caglayan, H.; Chen, J.; Xing, G.; Zheng, C.; Doan-Nguyen, V.; Kang, Y.; Engheta, N.; Kagan, C. R.; Murray, C. B. *ACS Nano* **2012**, *6* (3), 2804−2817.
(34) Loo, C.; Lin, A.; Hirsch, L.; Lee, M. H.; Barton, J.; Halas, N.; West, J.; Drezek, R. *Technol. Cancer Res. Treat.* **2004**, *3* (1), 33−40.
(35) Patsalas, P.; Logothetidis, S. *J. Appl. Phys.* **2001**, *90* (9), 4725−4734.
(36) CrysTec GmbH. http://www.crystec.de/daten/al2o3.pdf (accessed February 2013).
(37) Hirsch, L. R.; Stafford, R. J.; Bankson, J. A.; Sershen, S. R.; Rivera, B.; Price, R. E.; Hazle, J. D.; Halas, N. J.; West, J. L. *Proc. Natl. Acad. Sci. U.S.A.* **2003**, *100* (23), 13549−13554.
(38) Li, J.; Gao, L.; Sun, J.; Zhang, Q.; Guo, J.; Yan, D. *J. Am. Ceram. Soc.* **2001**, *84* (12), 3045−3047.
(39) Dekker, J. P.; van der Put, P. J.; Veringa, H. J.; Schoonman, J. *J. Mater. Chem.* **1994**, *4* (5), 689−694.
(40) Hu, J.; Lu, Q.; Tang, K.; Yu, S.; Qian, Y.; Zhou, G.; Liu, X. *J. Am. Ceram. Soc.* **2000**, *83* (2), 430−432.
(41) Giordano, C.; Erpen, C.; Yao, W.; Milke, B.; Antonietti, M. *Chem. Mater.* **2009**, *21* (21), 5136−5144.
(42) Calka, A. *Appl. Phys. Lett.* **1991**, *59* (13), 1568−1569.
(43) Takada, N.; Sasaki, T.; Sasaki, K. *Appl. Phys. A: Mater. Sci. Process.* **2008**, *93* (4), 833−836.
(44) Wisbey, A.; Gregson, P. J.; Tuke, M. *Biomaterials* **1987**, *8* (6), 477−480.
(45) Hyde, G. K.; McCullen, S. D.; Jeon, S.; Stewart, S. M.; Jeon, H.; Loboa, E. G.; Parsons, G. N. *Biomed. Mater.* **2009**, *4* (2), 025001.
(46) Williams, D. F. *Biomaterials* **2008**, *29* (20), 2941−2953.